

Real-time structural monitoring using the inverse Finite Element Method: A review of experimental applications in aerospace engineering

*Original*

Real-time structural monitoring using the inverse Finite Element Method: A review of experimental applications in aerospace engineering / Esposito, M.; Sorrenti, M.; Biscotti, V.; Gherlone, M.. - ELETTRONICO. - 1:(2025). ( 15th International Workshop on Structural Health Monitoring Stanford, California (USA) September 9 - 11, 2025).

*Availability:*

This version is available at: 11583/3003287 since: 2025-09-24T07:51:11Z

*Publisher:*

DEStech Publications

*Published*

DOI:

*Terms of use:*

This article is made available under terms and conditions as specified in the corresponding bibliographic description in the repository

*Publisher copyright*

(Article begins on next page)

# STRUCTURAL HEALTH MONITORING 2025

*Ensuring Mobility and Autonomy with Sustainability*

*Edited by*

**Fu-Kuo Chang**

*Department of Aeronautics and Astronautics  
Stanford University, Stanford, CA 94305*

**Alfredo Guemes**

*ETSI Aeronautics, Madrid, Spain*

Proceedings of the 15th International Workshop on Structural Health Monitoring  
Stanford University, Stanford, CA  
September 9-11, 2025

Sponsors:

• Office of Naval Research Science & Technology • Air Force Office of Scientific  
Research, United States Air Force • DEStech Publications, Inc.



**DEStech Publications, Inc.**

## **Structural Health Monitoring 2025**

DEStech Publications, Inc.  
439 North Duke Street  
Lancaster, Pennsylvania 17602 U.S.A.

Copyright © 2025 by DEStech Publications, Inc.  
All rights reserved

No part of this publication may be reproduced, stored in a retrieval system, or transmitted, in any form or by any means, electronic, mechanical, photocopying, recording, or otherwise, without the prior written permission of the publisher.

Printed in the United States of America  
10 9 8 7 6 5 4 3 2 1

Main entry under title:

Proceedings of the 15th International Workshop on Structural Health Monitoring 2025:  
Ensuring Mobility and Autonomy with Sustainability

AD EStech Publications book  
Bibliography: p.  
Includes index

ISBN No. 978-1-60595-699-2

# Real-Time Structural Monitoring Using the Inverse Finite Element Method: A Review of Experimental Applications in Aerospace Engineering

---

MARCO ESPOSITO, MATTEO SORRENTI,  
VINCENZO BISCOTTI and MARCO GHERLONE

## ABSTRACT

The realization of an efficient Structural Health Monitoring (SHM) system strongly depends on the availability of tools that can accurately detect the structural condition during operational life. This detection can be achieved by means of physical sensors, which can provide information on the mechanical state of a structure. However, the installation of several sensors is often impractical or even impossible for systems operating in complex environments, such as aerospace, marine, and civil structures. In this context, the inverse Finite Element Method (iFEM) was developed. This algorithm is based on the finite element discretization of the structural domain. iFEM is able to reconstruct two physical quantities crucial for assessing the health status of a structure, the displacement and the stress fields, from a reduced number of easily installable physical strain sensors and without the need to know the loading conditions and the material properties. The method is extremely accurate and computationally efficient. These characteristics make it suitable for the real-time monitoring of structures and crucial for feeding the SHM framework with sufficient data using only a few sensors installed. Several works have proved the method's accuracy when strain data are collected and processed offline. For the first time, this work presents an overview of the implementation of structural digital twins of several structures through the use of iFEM as a real-time monitoring system. In this study, both simple structures, such as a cantilevered beam, and more complex ones, such as a half-wing, are monitored live. In the presented applications, the data from the real structure is broadcast through an internet network so that the data from the sensors can feed the digital twin model remotely. These applications demonstrate that iFEM enables real-time monitoring, representing a significant step forward in the realization of the digital twin paradigm.

## INTRODUCTION

The structural maintenance of aerospace, civil, and marine structures is often complex and costly. Structural Health Monitoring (SHM) techniques help improve safety and reduce maintenance efforts [1]. In this context, the inverse Finite Element Method

(iFEM) was developed [2]. This monitoring algorithm uses easily obtainable discrete strain sensor data to reconstruct key structural responses such as displacements and stresses. The method is inspired by FEM and is based on a Finite Element modelization of the structure.

iFEM has been successfully applied to the monitoring of marine, civil, and aerospace structures [3–6]. However, in all the existing applications, the method has been applied off-line, i.e., data collected from the sensors have been post-processed to feed the algorithm at the end of the loading process. In this paper, real-time monitoring with iFEM is performed. The iFEM structural model is continuously fed with strain data, and the digital model is updated with the computed displacements at each time step. This procedure led to the realization of a proper structural digital twin.

The digital twin has been successfully implemented for two structures with an increasing level of complexity: a cantilevered aluminum beam and the half-wing of a commercial aero-model. Different communication systems between the sensors and the model are evaluated: serial communication is considered for the beam, whereas a Wi-Fi TCP/IP communication protocol is used for the half-wing. Moreover, for the half-wing, a recently developed formulation of iFEM, the Single Sensor Based iFEM (SSB-iFEM) [7], is tested. This formulation removes the standard iFEM requirement for back-to-back sensors, allowing the sensorization of thin-walled structures with single-sided sensor configurations.

The performed experimental tests on the two structures prove the impressive accuracy and efficiency of iFEM and SSB-iFEM. These characteristics allowed the two formulations to successfully implement a proper structural digital twin for structures with different features and sensor setups.

## IFEM AND SSB-IFEM FORMULATIONS

This section introduces the iFEM and its Single Sensor Based (SSB) enriched formulation. The iFEM is based on the discretization of the structural domain into finite elements (FE). It allows for the computation of the FE discretized displacement field of a deformed structure by minimizing, in a least-squares sense, a functional based on the error between the analytical and the experimental strains measured in some discrete locations on the structure. In its original formulation for shell elements [2], the iFEM error functional is not based directly on the *strain measurements*. Firstly, they must be converted into *strain measures*. The analytical strain measures are defined in the context of First-order Shear Deformation Theory for thin plates and shells as derivatives of the theory's kinematic variables (displacements and bending rotations) [8]. The top and bottom in-plane strain measurements and transverse shear measurements, respectively  $\boldsymbol{\varepsilon}_p^+$ ,  $\boldsymbol{\varepsilon}_p^-$ , and  $\boldsymbol{\varepsilon}_t$ , relate to the strain measures,  $e_k$ , through simple expressions:

$$\boldsymbol{\varepsilon}_p^+ = \begin{Bmatrix} \varepsilon_1 \\ \varepsilon_2 \\ \varepsilon_3 \end{Bmatrix} = \begin{Bmatrix} e_1 \\ e_2 \\ e_3 \end{Bmatrix} + t \begin{Bmatrix} e_4 \\ e_5 \\ e_6 \end{Bmatrix}, \boldsymbol{\varepsilon}_p^- = \begin{Bmatrix} \varepsilon_4 \\ \varepsilon_5 \\ \varepsilon_6 \end{Bmatrix} = \begin{Bmatrix} e_1 \\ e_2 \\ e_3 \end{Bmatrix} - t \begin{Bmatrix} e_4 \\ e_5 \\ e_6 \end{Bmatrix}, \boldsymbol{\varepsilon}_t = \begin{Bmatrix} \varepsilon_7 \\ \varepsilon_8 \end{Bmatrix} = \begin{Bmatrix} e_7 \\ e_8 \end{Bmatrix} \quad (1)$$

where  $t$  is half of the thickness of the structure, and the strain measures,  $e_k$ , are subdivided into membrane ( $k = 1, 2, 3$ ), bending ( $k = 4, 5, 6$ ), and transverse shear ones ( $k = 7, 8$ ). To compute the error functional associated with each inverse element, the

analytical strain measures are related to the nodal degrees of freedom (DOFs) of the element,  $\mathbf{u}^e$ , through proper shape function derivatives [9]. Similarly, Eq. 1 is used to compute the experimental strain measures,  $e_k^m$ , from the experimental strain measurements:

$$\begin{cases} e_1^m \\ e_2^m \\ e_3^m \end{cases} = \frac{1}{2} [(\boldsymbol{\varepsilon}_p^m)^+ + (\boldsymbol{\varepsilon}_p^m)^-], \quad \begin{cases} e_4^m \\ e_5^m \\ e_6^m \end{cases} = \frac{1}{2t} [(\boldsymbol{\varepsilon}_p^m)^+ - (\boldsymbol{\varepsilon}_p^m)^-] \quad (2)$$

This operation requires the back-to-back in-plane strain measurements,  $(\boldsymbol{\varepsilon}_p^m)^+$  and  $(\boldsymbol{\varepsilon}_p^m)^-$ , on the top and bottom surface of the corresponding inverse element. The resulting expression for the iFEM error functional is the following:

$$\Phi^e(\mathbf{u}^e) = \sum_{k=1}^8 w_k^e \lambda_k^e \int_{A^e} [e_k(\mathbf{u}^e) - e_k^m]^2 dA^e \quad (3)$$

where  $A^e$  is the area of the inverse element, the coefficient  $w_k^e$  guarantees the dimensional consistency between the strain measures [8], and the coefficient  $\lambda_k^e$  is used to account for sparse strain sensor configurations. It is set to 1 if the corresponding strain measure is measured, or to a small value ( $10^{-5}$ ) if it is not: for instance, since the transverse shear strains are not measurable through strain sensors, the values of  $\lambda_k^e$  for  $k = 7, 8$  are always set to  $10^{-5}$ .

To directly compare the SSB formulation to the original one, the SSB-iFEM functional is presented hereafter:

$$\Psi^e(\mathbf{u}^e) = \sum_{k=1}^8 (\lambda'_k)^e \int_{A^e} [\varepsilon_k(\mathbf{u}^e) - \varepsilon_k^m]^2 dA^e \quad (4)$$

It can be noticed immediately that the SSB formulation does not make use of the strain measures: the error is based on the strain measurements, and the eight terms that are summed in the functional are now related to the three components of the in-plane strain measurements, either on the top ( $k = 1, 2, 3$ ), or on the bottom ( $k = 4, 5, 6$ ) of the element, and to the transverse shear strain measurements ( $k = 7, 8$ ). Notably, as per Eq. 2, the transverse shear strain measures and the corresponding measurements coincide; thus, the related terms in the functionals are identical. On the contrary, the use of the in-plane measurements substantiates the difference between the two formulations. As the SSB-iFEM does not require the computation of the strain measures, single-sided sensor configurations are now employable: in such cases, similarly to the iFEM, the coefficients  $(\lambda'_k)^e$  corresponding to the unknown strain measurements are set to  $10^{-5}$ . For both iFEM and SSB-iFEM, the minimization of the error functional with respect to the nodal DOFs leads to a system of linear algebraic equations:

$$\frac{\partial \Phi^e(\mathbf{u}^e)}{\partial \mathbf{u}^e} = \mathbf{k}^e \mathbf{u}^e - \mathbf{f}^e = 0; \quad \frac{\partial \Psi^e(\mathbf{u}^e)}{\partial \mathbf{u}^e} = (\mathbf{k}^e)' \mathbf{u}^e - (\mathbf{f}^e)' = 0 \Rightarrow \text{Assembly} \Rightarrow \mathbf{K}\mathbf{U} = \mathbf{F} \quad (5)$$

To compute the vector of the global DOFs,  $\mathbf{U}$ , the local contributions of the element coefficient matrix,  $\mathbf{k}^e$  or  $(\mathbf{k}^e)'$ , and constant vector,  $\mathbf{f}^e$  or  $(\mathbf{f}^e)'$ , as in the standard FEM assembly procedure, are used to generate the system of linear global algebraic equations,

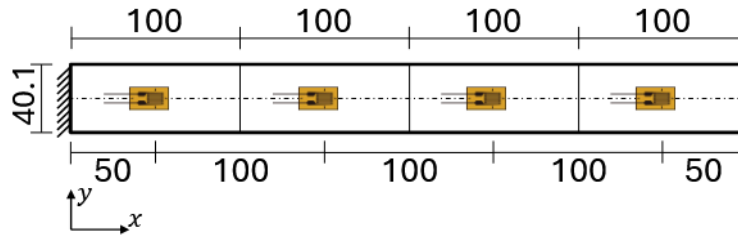


Figure 1. Geometry, iFEM discretization, and sensor configuration for the aluminum beam. All dimensions are expressed in mm.

where  $\mathbf{F}$  takes into account the mesh, the strain sensor configuration, and the values of the discrete strain measurements, whereas  $\mathbf{K}$  takes into account only the mesh and the strain sensor configuration. Therefore, it can be observed that the algebraic system is independent of the material properties and loading conditions of the structure and can be solved indifferently under static and dynamic loads. Moreover, it is important to highlight that the matrix  $\mathbf{K}$  does not change for a selected sensor configuration. This observation can be exploited to achieve the real-time monitoring of the displacement of a structure through iFEM and SSB-iFEM: the inversion of the matrix, which has a high computational cost, is performed only once. Thus, the real-time computation of  $\mathbf{U}$  is possible, as it requires only matrix-by-vector multiplications.

## ALUMINUM BEAM REAL-TIME MONITORING

In this work, two structures with different characteristics and sensorization schemes are analyzed to prove the versatility of iFEM. Furthermore, the two presented iFEM formulations best adapt to each of the selected test cases. Therefore, the live monitoring capabilities of iFEM are verified in different scenarios.

To demonstrate the live monitoring capabilities of iFEM, initially, a simple structure is used: a cantilevered aluminum beam made of 7075 T6 alloy, 3 mm thick. As highlighted in [7], the displacements of flat plate structures can only be reconstructed using the standard iFEM formulation, with a back-to-back configuration of strain sensors. Consequently, for this structure, eight mono-axial strain gauges are installed in a back-to-back layout to measure the axial strain along the x-direction in four locations. The beam geometry and sensor layout are shown in Fig. 1. The iFEM discretization is also presented in Fig. 1. It consists of 4 iQS4 elements with a total of 10 nodes.

For this application, the strain data are recorded through an acquisition system based on Arduino and Hx711 A/D 24-bit converters developed for this experiment. This system is connected and shares the sensors' data with a computer through a serial communication port. On the computer, the standard iFEM algorithm is implemented and fed with the strain data in real-time.

The beam is clamped on one end during the experiment, and transverse loads are applied manually at various points along the beam. The strain data, acquired at a frequency of 50 Hz, are processed with the standard iFEM to reconstruct the displacements and, from them, the stress fields. In the animated figure 2, it is possible to watch some extracted frames from the experiment. The entire experiment video can be watched at <https://youtu.be/UZSije1ikhw>. The system is responsive and accurate, with no notice-

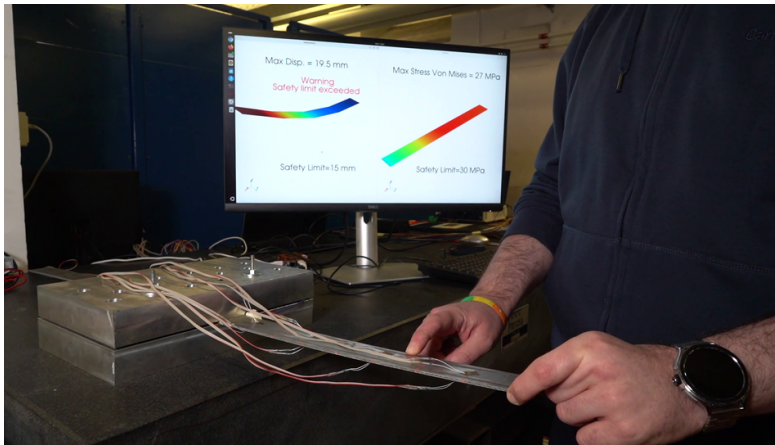


Figure 2. Real-time monitoring of displacements and stresses on the aluminium beam. The animated figure can only play on Adobe Acrobat Reader®.

able reconstruction delay.

## HALF-WING REAL-TIME MONITORING

The second experiment is a more complex one that is performed to demonstrate the impressive versatility of SSB-iFEM. The monitored structure is the half-wing of a commercial hotliner produced by the Robbe modelsport company, Fig. 3. More specifically, the selected one is the "Limit PRO" hotliner, with a Glass-Fiber-Reinforced Polymer/Carbon-Fiber-Reinforced Polymer (GFRP/CFRP) structure. This test is particularly significant since it focuses on a commercial product, and the manufacturer has not released information on the geometry and material characteristics. Moreover, the internal surfaces of the half-wing are not accessible. For these reasons, the recently formulated SSB-iFEM represents the only feasible choice for the monitoring. In fact, the method allows for the sensorization of the thin-walled structure's sole external surface, widening the standard iFEM's applications. Moreover, although the material properties are not known, both the iFEM and the SSB-iFEM can still perform the displacement and strain field reconstruction, as only the geometrical properties of the structure are needed. The geometrical features were derived through a reverse engineering process employing computed tomography. The data retrieved through this process are summarized in Fig. 4, and include the thickness of the skin,  $t = 1.45 \text{ mm}$ . No information about the internal wing-box is presented, as it is not needed to reconstruct the whole displacement field of the half-wing outer shape.

Fig. 4 also shows the strain sensor configuration adopted for the application. In this case, fiber optic distributed strain sensors based on the Rayleigh back-scatter principle are used. In particular, six measuring lines along the wingspan are installed by means of a unique optical fiber. Three lines are placed on the upper surface and three on the lower surface of the half-wing. The adopted fiber sensor has a high density of sensing locations on the fiber, which enables the sensorization of all the elements of the inverse mesh (Fig. 4) that lie underneath the sensor.

The first analysis performed on the specimen is a static test to validate the accuracy of the SSB-iFEM for this application. This test is performed by applying a concentrated

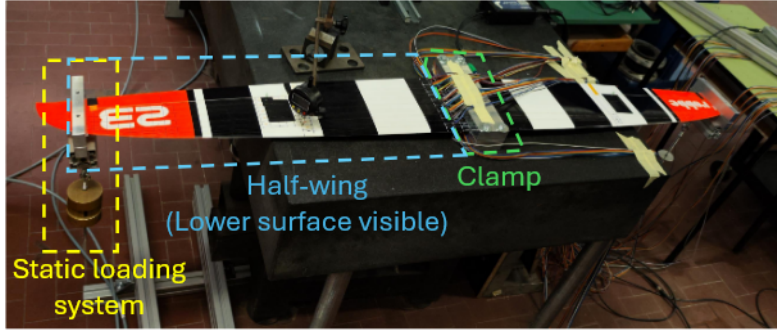


Figure 3. Half-wing experimental configuration.

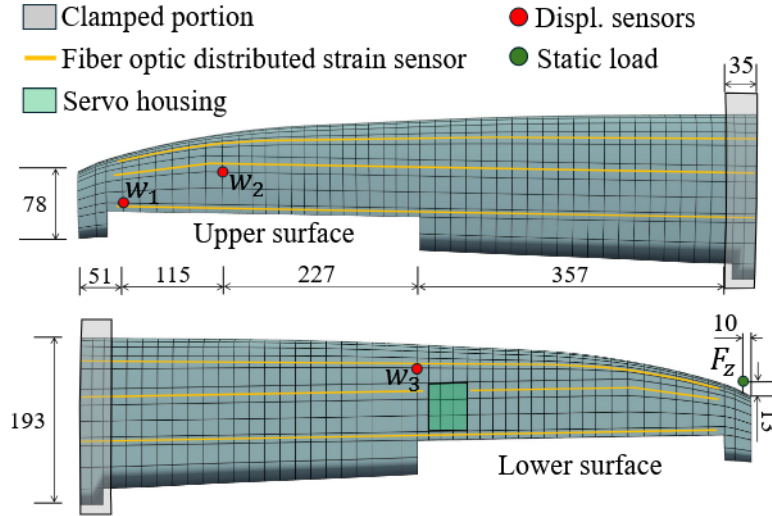


Figure 4. Half-wing geometry, iFEM discretization, and sensor configuration. All dimensions are expressed in mm.

transverse load  $F_z$  at the tip of the wing (Figs. 3 and 4). The root of the wing is clamped through aluminum blocks fixed on a test bench. The structure is mounted upside down, so that the application of the weights generates a load that is in the same direction as the lift in operative conditions. To assess the accuracy of the displacement reconstruction, two transverse deflections ( $w_1$ ,  $w_2$ ) of the wing are measured on the upper surface of the half-wing employing two time-of-flight laser sensors. One deflection ( $w_3$ ), on the lower surface, is measured with an LVDT. The sensors are distributed on the surfaces as shown in Fig. 4. The static test results are reported in Table I and show very accurate reconstruction of the measured displacements, with errors that do not exceed 5.6% and that are very small (1.1%) for the maximum measured displacement, i.e.,  $w_1$ .

	Exp. values	SSB-iFEM	%ERR
$w_1$ [mm]	18.34	18.15	-1.1%
$w_2$ [mm]	12.35	12.02	-2.7%
$w_3$ [mm]	4.85	4.59	-5.6%

TABLE I. Static test results for  $F_z = 2.0$  Kg.

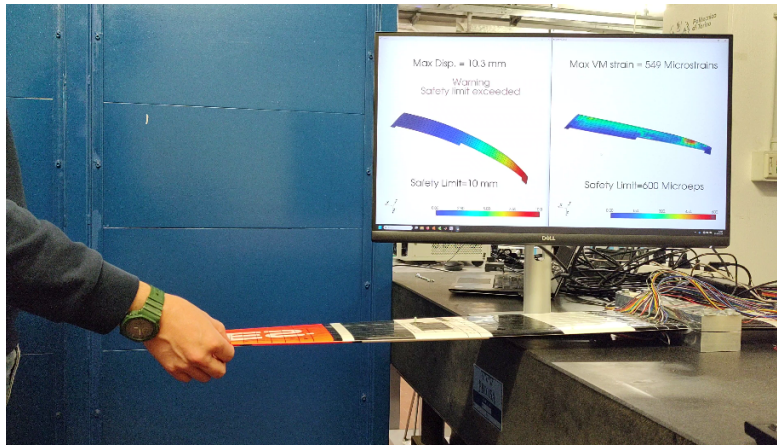


Figure 5. Real-time monitoring of displacements and strains on the half-wing. The animated figure can only play on Adobe Acrobat Reader®.

Once the method's accuracy is verified, its real-time capabilities are tested. This test case represents a more challenging application with respect to the aluminum beam for multiple reasons. The inverse model of the structure consists of 941 elements and 994 nodes. The model size has an impact on the computational cost for real-time reconstructions. Moreover, the amount of information from the strain sensors is sensibly higher and requires a significant data exchange between the sensing and computing systems. For this experiment, the communication system between the sensors and the computer running SSB-iFEM is more complex. The strain data from the fiber sensors are acquired using a Luna ODISI 6100 acquisition system. The data are then streamed to the computing system through a Wi-Fi TCP/IP protocol, and the data packets are elaborated in real-time to reconstruct the displacement and strain field with SSB-iFEM. The stresses cannot be computed since the material characteristics are not disclosed for this application. The Von Mises strains are computed and plotted together with the displacement field, instead. The test is run using the maximum acquisition frequency of the ODISI 6100 system, i.e., 12.5 Hz. This limit is imposed by the acquisition system technology, and not by SSB-iFEM or the computing system. The final result of the real-time monitoring, when loading the wing dynamically by hand, is shown in the animated Fig. 5. A more detailed video of the experiment can be seen at <https://youtu.be/xV8KFxSgB0A>. The video proves the realization of a structural digital twin for a representative aerospace commercial structure.

## CONCLUDING REMARKS

This paper presents two experimental applications of the inverse Finite Element Method (iFEM) for the real-time monitoring of structures. Two test cases and two different formulations of the iFEM are considered. The first test case is a simple one, a cantilevered aluminum beam, and is analyzed using the standard iFEM formulation. The second experiment consists of the real-time monitoring of the half-wing of a commercial hotliner aero-model. For this application, a novel iFEM formulation, the SSB-iFEM, is used. This formulation allows for the sensorization of the structure with sensors on one surface only, removing the constraint of back-to-back sensor configurations. The two

experiments show that the iFEM is computationally efficient in both its formulations and can manage the real-time monitoring of simple and complex structures receiving streaming data from different sensors via different communication protocols. For both experiments, a structural digital twin is successfully realized with iFEM.

## ACKNOWLEDGMENT

Vincenzo Biscotti acknowledge the support of the Italian Ministry of University and Research and the Sustainable Mobility Center through the project PNRR - M4C2 - CNMS - Spoke 1, funded under the scheme CN00000023 - PNRR – M4C2 Inv. 1.4 with grant agreement num. 55\_PRR22\_1155\_22\_GG002138. The authors gratefully acknowledge the Fondazione Compagnia di San Paolo for supporting this research activity by funding the DIMOSS project in the framework of the PoC Instrument 2022/2024, cut-off 3.

## REFERENCES

1. Farrar, C. R. and K. Worden. 2007. “An Introduction to Structural Health Monitoring,” *Philosophical Transactions of the Royal Society A: Mathematical, Physical and Engineering Sciences*, 365(1851):303–315, ISSN 1364503X, doi:<https://doi.org/10.1098/rsta.2006.1928>.
2. Tessler, A. and J. L. Spangler. 2005. “A least-squares variational method for full-field reconstruction of elastic deformations in shear-deformable plates and shells,” *Computer Methods in Applied Mechanics and Engineering*, 194:327–339, ISSN 00457825, doi:10.1016/j.cma.2004.03.015.
3. Kefal, A. 2019. “An efficient curved inverse-shell element for shape sensing and structural health monitoring of cylindrical marine structures,” *Ocean Engineering*, 188:106262, ISSN 0029-8018, doi:<https://doi.org/10.1016/j.oceaneng.2019.106262>.
4. Wang, J., L. Ren, R. You, T. Jiang, Z. Jia, and G. xin Wang. 2021. “Experimental study of pipeline deformation monitoring using the inverse finite element method based on the iBeam3 element,” *Measurement*, 184:109881, ISSN 0263-2241, doi:<https://doi.org/10.1016/j.measurement.2021.109881>.
5. Miller, E. J., R. Manalo, and A. Tessler. 2016. “Full-Field Reconstruction of Structural Deformations and Loads from Measured Strain Data on a Wing Using the Inverse Finite Element Method,” Report NASA/TM-2016-219407, NASA; Edwards, CA United States.
6. Oboe, D., L. Colombo, C. Sbarufatti, and M. Giglio. 2021. “Shape sensing of a complex aeronautical structure with inverse Finite Element Method,” *Sensors*, 21(4), ISSN 1424-8220, doi:10.3390/s21041388.
7. Biscotti, V., M. Esposito, and M. Gherlone. 2025. “A new Single Sensor Based iFEM formulation for shape-sensing of thin-walled structures instrumented with single-sided sensor configurations: Formulation, numerical assessment, and experimental validation,” *Mechanical Systems and Signal Processing*, 232:112700, ISSN 0888-3270, doi:<https://doi.org/10.1016/j.ymsp.2025.112700>.
8. Esposito, M., M. Mattone, and M. Gherlone. 2022. “Experimental Shape Sensing and Load Identification on a Stiffened Panel: A Comparative Study,” *Sensors*, 22, ISSN 14248220, doi:10.3390/s22031064.
9. Kefal, A., E. Oterkus, A. Tessler, and J. L. Spangler. 2016. “A quadrilateral inverse-shell element with drilling degrees of freedom for shape sensing and structural health monitoring,” *Engineering Science and Technology, an International Journal*, 19:1299–1313, ISSN 22150986, doi:10.1016/j.jestch.2016.03.006.